Available online at www.sciencedirect.com
SCIENCE DIRECT
Global and Planetary Change 52 (2006) 121–141
GLOBAL AND PLANETARY CHANGE
www.elsevier.com/locate/gloplacha

Modeling mineral dust emissions from Chinese and Mongolian deserts

B. Laurent [a,*], B. Marticorena [a], G. Bergametti [a], F. Mei [b]

[a] *Laboratoire Interuniversitaire des Systèmes Atmosphériques, Universités Paris VII-XII, UMR CNRS 7583, 61 avenue du Général de Gaulle, F-94010 Créteil Cedex, France*
[b] *Xi'an University of Engineering Science and Technology, Jinhua South Road 19#, 710048, Xi'an, China*

Accepted 9 February 2006
Available online 6 May 2006

Abstract

The present study investigates the frequency and intensity of mineral dust emissions over the deserts of eastern Asia from 1996 to 2001. Mineral dust emissions are simulated using a physical dust emission scheme over a region extending from 35.5°N to 47°N and from 73°E to 125°E. The input parameters required by the dust emission model are (1) surface features data including aerodynamic roughness length, soil dry size distribution and texture; and (2) meteorological surface data, mainly wind speed, soil moisture and snow cover. The way by which these surface features and meteorological data can be assessed is described and discussed. The influence of soil moisture and snow cover is taken into account and their effects on simulated dust emission are quantified.

The simulations reproduce on a daily basis the location and intensity of the severe events of April 1998 and spring 2001 as recorded by the meteorological stations and/or described in various studies. Based on 6 yr of simulations, the main dust source regions are identified and their relative contributions to the total dust emissions are quantified.

The seasonal cycle of the dust storms frequency is well reproduced with a maximum in spring. The simulations suggest that it is mainly controlled by the emissions occurring in the Taklimakan desert in latter spring and in summer, and by those occurring in the northern deserts of China in winter. The Taklimakan desert appears to be the most frequent and steady source of dust emissions during the studied period. On the other hand, in the Gobi desert, only a few dust emission events are simulated, but the dust amount emitted during each event is generally very large. In the northern deserts of China, dust emissions are frequent and their intensity is variable.

These results show an important annual and inter-annual variability of the emitted dust (between 100 Mt yr^{-1} and 460 Mt yr^{-1}), mainly controlled by the occurrence of severe events in the Gobi desert and in the northern deserts of China.

Keywords: mineral dust; Asian dust emissions; roughness length; soil size distribution

1. Introduction

Chinese and Mongolian deserts are among the major sources of mineral dust. Dust storms originating from these desert regions are mainly caused by frontal activities and prevail mostly during spring (Merrill et

* Corresponding author.
E-mail addresses: blaurent@lisa.univ-paris12.fr (B. Laurent), marticorena@lisa.univ-paris12.fr (B. Marticorena), bergametti@lisa.univ-paris12.fr (G. Bergametti), meifanmin@xaist.edu.cn (F. Mei).

0921-8181/$ - see front matter © 2006 Elsevier B.V. All rights reserved.
doi:10.1016/j.gloplacha.2006.02.012

al., 1989; Qian et al., 2002). When looking at the number of dust storms recorded in China since 1960, it appears that the occurrence of dust storms was twice more frequent during the period 1960–1984 than during the period 1984–1997 (Zhang et al., 2003). However, between 1997 and 2002, the records suggest a significant increase in the number of dust storms occurring during spring in China (Zhang et al., 2003). This increase is particularly noticeable in the deserts of northern Asia (Kurosaki and Mikami, 2003). Moreover, large areas of ongoing desertification due to land use have been identified in China (Mainguet, 1996; Xue, 1996; Zha and Gao, 1997) and Mongolia (Natsagdorj et al., 2003) and may constitute additional dust sources.

Dust emissions and their transport from the Asian desert regions have been investigated using numerical and modelling approaches (Wang et al., 2000; Uno et al., 2001; Gong et al., 2003; Shao et al., 2003; Zhang et al., 2003; Zhao et al., 2003). In particular, detailed dust emission schemes have been recently used to simulate and forecast the mineral dust emissions and its transport over China (Gong et al., 2003; Shao et al., 2003). However, the specificities of the various regions in terms of surface features are generally not completely taken into account due to the lack of precise information. Recently, Laurent et al. (2005) used a satellite derived roughness map to improve the estimates of erosion thresholds in the Chinese and Mongolian deserts. The 3-yr simulations, performed by these authors, also include the effect of soil moisture and snow cover on dust emission frequencies. However, these simulations are limited to an estimate of the dust emission frequencies but no quantitative assessment of the emitted dust masses is provided.

The present study is a continuation of the work of Laurent et al. (2005) and is based on a similar modelling approach. However, to provide a quantitative estimate of dust emissions, a specific database for the soil size distributions and textures is derived from in-situ measurements (Ding et al., 1999; Yang et al., 2001; Mei et al., 2004). Furthermore, the simulations are extended over the period from 1996 to 2001 for which the meteorological records suggest a significant increase of the number of dust storms (Zhang et al., 2003).

After a brief summary of the dust emission model, the surface and meteorological parameters are described, with a special focus on the soil size distributions. Simulations for well-documented events are first discussed and compared to available data, in particular to the horizontal visibility recorded in Chinese and Mongolian meteorological stations. The 6-yr simulations of dust emissions are used to investigate the seasonality and the inter-annual variability of the main dust sources.

2. Dust emission model

2.1. Principle of dust emission

Mineral dust emissions by wind in arid areas are a non-linear process, depending both on the surface features and meteorological conditions. The emission of transportable soil-derived particles is a power function of the wind friction velocity, U^*, but occurs only when a threshold value, U_t^*, has been reached. This erosion threshold mainly depends on the soil size distribution, on the roughness induced by the presence of non-erodible elements over the erodible surface and on the soil moisture. Once the erosion threshold is reached, the soil grains enter into a horizontal movement called saltation. Sandblasting, or bombardment, is the main dust production process. It refers to the release of fine dust particles by impact of soil particles on the surface and/or breakage of soil aggregates. The saltating soil grains provide the kinetic energy required to exceed the cohesive forces linking the dust particles to the soil aggregates.

The total amount of material mobilized by wind, or horizontal flux (G), mainly depends on the wind friction velocity and on the soil size distribution, while the intensity of the dust flux, i.e., vertical flux (F), is influenced by the ability of the soil to release fine transportable particles (Gillette, 1979; Shao et al., 1993).

All three processes (erosion threshold, saltation and sandblasting) are explicitly parameterized in the dust emission scheme developed and validated by Marticorena and Bergametti (1995) and Marticorena et al. (1997a,b). The input parameters required for a large-scale application of this physical scheme and the way they can be retrieved are fully described in Marticorena et al. (1997a) and Callot et al. (2000).

2.2. Dust emission model parameterizations

2.2.1. Erosion threshold

Briefly, the dust emission model is based on a parameterization of the threshold wind friction velocity as a function of (1) the size of the in-place erodible aggregates (D_p), (2) the aerodynamic roughness length of the overall surface (Z_0) and (3) the aerodynamic roughness length of the erodible part of the surface (z_{0s}).

The size dependence of the erosion threshold is an adaptation of the parameterization proposed by Iversen and White (1982). The influence of the surface

roughness length is accounted for using a drag partition scheme developed by Marticorena and Bergametti (1995).

$$U_t^*(D_p, Z_0, z_{0s}) = \frac{U_t^*(D_p)}{f_{eff}(Z_0, z_{0s})} \quad (1)$$

$$\text{with } f_{eff}(Z_0, z_{0s}) = 1 - \left(\left(\frac{Z_0}{z_{0s}}\right) / \left(0.35 \left(\frac{10}{z_{0s}}\right)^{0.8}\right)\right) \quad (2)$$

D_p, Z_0 and z_{0s} having units of centimeters.

This parameterization reproduces satisfyingly the wind-tunnel measurements of erosion threshold wind friction velocities performed over various natural surfaces (Gillette, 1981; Nickling and Gillies, 1989).

The increase of the erosion threshold wind velocities due to soil moisture w is computed according to Fécan et al. (1999) as a function of the soil residual moisture w' (Eqs. (3) and (4)), which is the soil moisture that must be reached to increase the erosion threshold.

$$\text{for } w < w' : \quad \frac{U_{tw}^*}{U_{td}^*} = 1 \quad (3)$$

$$\text{for } w > w' : \quad \frac{U_{tw}^*}{U_{td}^*} = \left[1 + 1.21(w - w')^{0.68}\right]^{0.5} \quad (4)$$

with w' depending on the soil clay content:

$$w' = 0.0014(\%\ \text{clay})^2 + 0.17(\%\ \text{clay}) \quad (5)$$

w and w' having units of % (mass of water/mass of dry soil).

2.2.2. Erosion and dust fluxes

2.2.2.1. Horizontal flux. Including the size-dependent expression of the threshold wind friction velocity in a formulation of the horizontal flux (G) (White, 1979) provides a size-dependent equation. This equation allows the computation of the amount of material mobilized by wind and its size distribution as a function of the wind friction velocity:

$$G = E\frac{\rho_a}{g}U^{*3}\sum_{D_p}\left(1 + \frac{U_t^*(D_p, Z_0, z_0)}{U^*}\right) \times \left(1 - \frac{U_t^*(D_p, Z_0, z_0)^2}{U^{*2}}\right) dS_{rel}(D_p)\, dD_p \quad (6)$$

where E is the fraction of erodible to total surface, $dS_{rel}(D_p)$ is the relative surface covered by the particles of diameter D_p.

This size-dependent representation of the horizontal flux reproduces well the total mass and size distribution of the horizontal fluxes measured in wind-tunnel for various soil substrates and wind friction velocities by Williams (1964) or Sörensen (1985). However, it must be noted that such a parameterization does not correctly reproduce the horizontal flux for supply-limited surfaces such as crusted soils (Lopez, 1998).

2.2.2.2. Dust vertical flux. Only physically explicit sandblasting models such as those developed by Alfaro and Gomes (2001) or by Shao et al. (2003) allow both the simulation of the mass and of the size distribution of the emitted dust. However, it has been shown (In and Park, 2002; Gong et al., 2003; Shao et al., 2003) that these physical models are highly sensitive to the input soil size distribution. Since these soil size distributions are only poorly known (see Section 3.1.2) in arid areas, using such sandblasting models could lead to large uncertainties in the simulations of the dust size distributions and masses. We thus decide to use the parameterization developed by Marticorena and Bergametti (1995) less sensitive to the accuracy of the soil size distribution.

Based on Gillette's (1979) coupled measurements of horizontal fluxes (G) and vertical fluxes of dust particles with a diameter <20 μm (F), Marticorena and Bergametti (1995) established an empirical relationship linking the ratio of the dust flux to the horizontal flux, i.e., the sandblasting efficiency α, to the soil clay content:

$$\alpha = \frac{F}{G} = 10^{(0.134(\%\ \text{clay}) - 6)}. \quad (7)$$

To summarize, the model used in this study allows us to compute the dust flux provided that the required surface and meteorological input parameters have been determined. More details on the physical dust emission model can be found Marticorena and Bergametti (1995) and Marticorena et al. (1997a).

3. Input parameters

3.1. Surface parameters

3.1.1. Aerodynamic roughness length

Marticorena et al. (2004) investigated the possibility to retrieve the surface roughness of arid areas using the surface bi-directional reflectance products derived from the POLarization and Directionality of the Earth Reflectance (POLDER-1) space-borne. An empirical

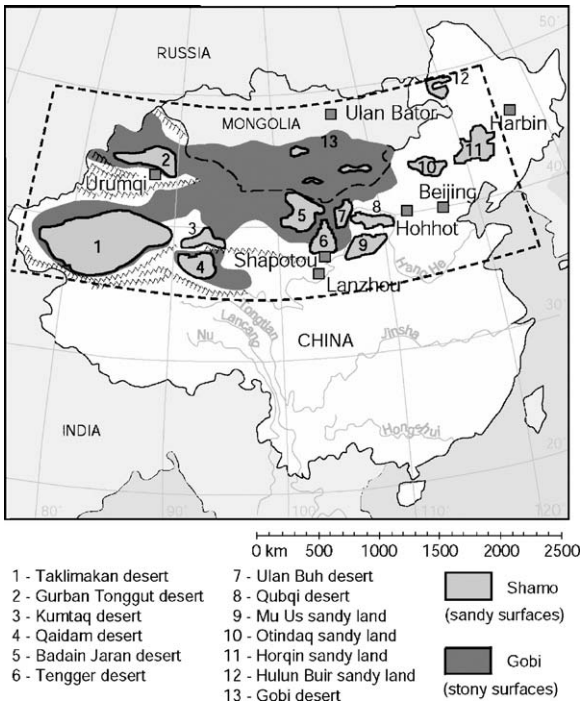

Fig. 1. Desert and desertified areas of China and Mongolia (adapted from Mitchell and Fullen, 1994; Sun et al., 2001); (- - -) studied area.

relationship between the aerodynamic roughness length and the so-called protrusion coefficient (PC) derived from the POLDER-1 bi-directional reflectance distribution function in the visible range was established. When applied over the Sahara and the Arabian Peninsula, this method leads to a good agreement between simulated dust event frequencies and those derived from Infrared Meteosat Dust Index (IDDI) (Marticorena et al., 2004). Laurent et al. (2005) applied this method to eastern Asia and established a composite map of PC over a region (35.5°N to 47°N and 73°E to 125°E) including the main identified desert areas of China and Mongolia (Fig. 1). This allows the authors to derive a map of aerodynamic roughness length for the Chinese and Mongolian arid areas with a spatial resolution of 1/4° × 1/4° (Fig. 2). The roughness lengths retrieved vary at least over three orders of magnitude (from less than 10^{-2} mm in sandy areas of the Taklimakan desert up to 5 mm in some parts of the Gobi desert). The aerodynamic roughness lengths retrieved over gobi surfaces range typically from 0.34 to 0.64 mm, in agreement with roughness length measurements over gobi surfaces in northern China (Gansu Province) (from 0.3 to 1.9 mm for sandy gobi, sand-gravel gobi and gravel gobi) (Xian et al., 2002). For similar surfaces, the retrieved values are also in agreement with the roughness lengths measured either from field (Greeley et al., 1997) or wind-tunnels (Gillette et al., 1982; Mc Kenna-Neuman and Nickling, 1994; Marticorena et al., 1997b) experiments.

3.1.2. Soil size distribution and texture

Two major soil characteristics are accounted for in the dust emission model: (1) the soil size distribution representing the size of the in situ erodible grains and aggregates and (2) the soil texture (see Section 2).

Soil maps generally classify soils according to the well-known textural triangle defined by the three size components: sand (2000 to 80 or 63 μm), silt (80 or 63 to 4 or 2 μm) and clay (<4 or 2 μm) (Chatenet et al., 1996; Ding et al., 1999). However, loose clay particles are generally not encountered in the natural soils. They generally form aggregates of larger size. Thus, they can be determined only by wet sedimentation techniques (ultrasonic pretreatment, dissolution), which break these aggregates (Chatenet et al., 1996; Ding et al., 1999). As a result, such a classification cannot be directly used to

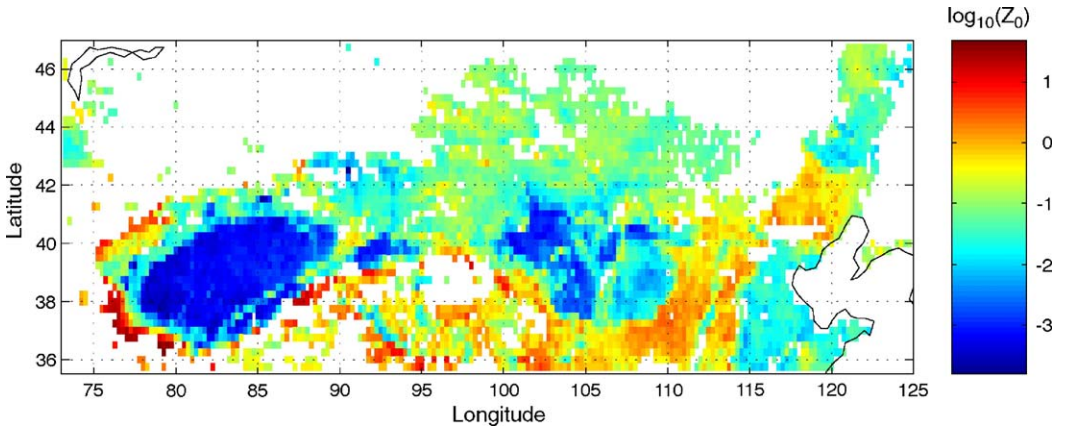

Fig. 2. Map of the logarithm of the aerodynamic roughness length Z_0 with a spatial resolution of 1/4° × 1/4° (Z_0 is in cm).

characterize the in-situ size distributions of erodible soils. An alternative approach is to determine the size distribution of the soil using dry techniques that minimize the breakage of the aggregates. Such an approach has been proposed by Chatenet et al. (1996) and applied to Chinese soil samples by Mei et al. (2004).

3.1.2.1. Chinese soil grain size distributions. Based on an intensive sampling of the main Chinese arid areas, Mei et al. (2004) determined the typical micro-aggregated size distribution of surface soil. Following Chatenet et al. (1996), the soil mass size distribution was determined by dry sieving using 10 size classes (<40 μm, 40–63 μm, 63–80 μm, 80–100 μm, 80–100 μm, 100–125 μm, 125–250 μm, 250–500 μm 500–800 μm, 800–1000 μm, 1000–2000 μm) for each surface sample. A fitting procedure (Gomes et al., 1990) based on the adjustment of 2 lognormal modes to the soil mass measured in the various size classes was then used. This procedure, which provides mass median diameter (MMD_i), standard deviation (σ_i) and mass fraction (P_i) of each of the two populations, was applied to the individual samples from Mei et al. (2004) for each of the sampled desert areas: Inner Mongolia, Gurban Tonggut desert, East of Xinjiang area, Ulan Buh desert, Mu Us desert, Taklimakan, Hexi Corridor, Tengger desert and Horqin sandy land.

For the whole data set (Table 1), except the Horqin sandy land, the median values of the MMD_1 (i.e., of the finer population) are remarkably comparable (~90 μm) not only for the various samples of a given desert as indicated by the low standard deviations, but also from one desert area to another. On the contrary, the median diameters of the coarser mode, MMD_2, exhibit higher standard deviations for each desert area and differ from one desert to another. Once again, the samples from the Horqin sandy land exhibit a median MMD_2 much higher than the other desert areas. It must be noted that both the fine and coarse modes of the Chinese desert soils are significantly finer than the ones estimated for the Sahara (Chatenet et al., 1996), but comparable to the ones observed in North America, i.e., for similar latitude and thus comparable weathering conditions (Marticorena et al., 1997b).

The median mass fraction of the fine and coarse modes, P_1 and P_2, vary significantly from one desert to another (Table 1). The finer modes are dominant for the Taklimakan desert, the Horqin sandy land and the Tengger desert. The standard deviation of P_i can reach 31% in the Tengger desert but it does not exceed 19% in the other desert areas. When the finer mode is not dominant, P_1 varies from 29% to 42%.

Due to the variations of the coarse mode diameter and of the mass fractions of the two modes, it was not possible to determine typical size distributions for the whole studied area. However, the standard deviations of the statistical parameters, characterizing the size distributions, are generally low enough to consider the median values from Table 1 as representative of each

Table 1
Median and standard deviations of the statistical parameters of the log-normal distributions (MMD_i, σ_i and P_i), and clay, silt and sand contents for the soil samples collected in desert areas of China by Mei et al. (2004). *n* indicates the number of samples collected in each desert area

		MMD_1 (μm)	σ_1	P_1 (%)	MMD_2 (μm)	σ_2	P_2 (%)	% Clay (0–2 μm)	% Silt (2–50 μm)	% Sand (50–2000 μm)
Inner Mongolia	Median	86	1.38	42	457	1.74	58	11.9	34.1	53.0
n=21	S.D.	7	0.20	17	30	0.34	17	3.9	13.2	16.4
Gurban Tunggut	Median	94	1.12	36	170	1.69	64	3.6	13.5	82.0
n=3	S.D.	5	0.07	19	162	0.26	19	7.5	40.3	47.8
Est of Xinjiang	Median	90	1.24	29	293	1.66	71	9.9	34.7	55.3
n=4	S.D.	10	0.27	15	125	0.09	15	6.6	17.7	24.2
Ulan Buh	Median	97	1.30	52	316	1.59	48	3.4	8.6	88.2
n=10	S.D.	5	0.10	13	157	0.35	13	0.7	1.8	2.3
Mu Us	Median	99	1.17	35	330	1.37	65	1.6	7.7	90.2
n=8	S.D.	13	0.12	11	88	0.23	11	0.7	2.5	2.6
Taklimakan	Median	84	1.34	97	442	1.42	3	2.0	10.7	87.8
n=12	S.D.	21	0.24	12	185	0.44	11	1.1	14.0	14.8
Hexi Corridor	Median	97	1.26	40	386	1.59	60	4.8	14.8	80.6
n=10	S.D.	28	0.41	11	123	0.34	11	6.7	30.5	36.6
Tengger	Median	120	1.48	72	322	1.29	28	2.6	7.3	90.7
n=9	S.D.	38	0.26	31	98	0.28	31	1.4	5.1	6.4
Horqin	Median	315	1.29	100	773	1.16	0	–	–	–
n=23	S.D.	138	0.12	3	40	0.14	3	–	–	–

desert area. These results also show that the soil size distribution of a desert area can hardly be determined a priori without experimental evidences.

Some arid areas, such as the Badain Jaran and Qubqi desert or the Otin Daq and Hulun Buir sandy lands, have not been sampled by Mei et al. (2004). Additional information on the dry soil size distribution of Chinese desert areas was found in Yang et al. (2001). These authors provide an average sand size distribution for a larger number of arid areas of China than Mei et al.'s (2004), but the size distribution is given for only five size classes. Moreover, the resolution is poor in the particle size range 100–700 μm in which the mass median diameters previously determined are all included. However, these additional data can be used to identify similarities in soil size distributions between the different desert areas. Typically, the Badain Jaran desert exhibits similar sand size distribution to its neighbor Ulan Buh desert, while the Qubqi desert exhibits a soil size distribution comparable to the Tengger desert. Since the soil size distributions of the Ulan Buh and Tengger deserts were determined with a higher confidence level using the data from Mei et al. (2004), they have been assigned respectively to the Badain Jaran and Qubqi deserts. The Otin Daq and Hulun Buir sandy lands are desertified areas, like the Horqin sandy land, and they are located in the same geographical area. Consequently, the soil size distribution of the Horqin sandy land derived from Mei et al. (2004) samples was assigned to these two sandy lands.

Both Yang et al. (2001) and Mei et al. (2004) also tried to document the soil size distribution of gobi surfaces, i.e., surfaces covered with gravel and pebbles. Mei et al. (2004) sampled gobi surfaces in Inner Mongolia, while Yang et al. (2001) provided measurements from alluvial and delluvial gobi surfaces in the vicinity of Dunhuang and Yumen. For this type of surface, these two data sets exhibit comparable mass size distributions. However, Mei et al.'s (2004) the soil size distributions, based on a larger number of size classes, can be considered as more precise. Thus, the median soil size distribution obtained for Inner Mongolia (Table 1) has been assigned to all gobi surfaces.

The studied area also includes potentially erodible surfaces that are not identified as desert areas, like the Loess Plateau. For these regions, we derived the statistical parameters of the soil size distribution from the average size distribution of loess and sandy loess from Yang et al. (2001).

Table 2 summarizes the statistical parameters of the different soil size distributions used in this work. Each identified desert is characterized by a soil size distribution derived from in situ measurements. The gobi surfaces are identified using the roughness length as a criterion. Once the roughness length derived from POLDER-1 observations is higher than 0.5 mm, i.e., the roughness lengths typically measured over Chinese gobi surfaces (Xian et al., 2002), the surface is considered as a gobi surface. The sandy loess and loess areas are crudely located based on geographical considerations.

3.1.2.2. Smooth roughness length. Following Marticorena et al. (1997a), the smooth roughness length, z_{0s}, is assumed to be 1/30 of the coarser mass median diameter of the soil size distribution, except if the roughness length derived from POLDER-1 is lower

Table 2
Statistical parameters of the soil size distributions, smooth roughness lengths (z_{os}), ratio of the dust flux to saltation flux (α) and residual soil moisture (w') assigned to the different desert areas of China and Mongolia

	Population 1			Population 2			z_{os} (10^{-3} cm)	α (cm^{-1})	w'
	MMD_1 (μm)	σ_1	P_1 (%)	MMD_2 (μm)	σ_2	P_2 (%)			
Gobi (Inner Mongolia)[a]	86	1.38	42	457	1.74	58	1.52	3.93E−05	2.22
Loess area[b]	65	1.28	100	–	–	–	0.22	1.90E−04	3.29
Sandy Loess area[b]	74	1.17	100	–	–	–	0.25	1.90E−04	3.29
Taklimakan and Kumtaq[a]	84	1.34	97	442	1.42	3	0.28	1.85E−06	0.35
Ulan Buh and Badain Jaran[a]	97	1.30	52	316	1.59	48	1.05	2.85E−06	0.59
Tengger and Kubqi[a]	120	1.48	72	322	1.29	28	1.07	2.23E−06	0.45
Mu Us[a]	99	1.17	35	330	1.37	65	1.10	1.64E−06	0.28
Horqin[a]	315	1.29	100	–	–	–	1.05	1.64E−06	0.28
East of Xinjiang area[a]	90	1.24	29	293	1.66	71	0.98	2.12E−05	1.82
Hexi Corridor[a]	97	1.26	40	386	1.59	60	1.29	4.40E−06	0.85
Gurban Tunggut[a]	94	1.12	36	170	1.69	64	0.57	3.04E−06	0.63

[a] From Mei et al. (2004).
[b] From Yang et al. (2001).

(Table 2). For the Taklimakan desert, the coarser population represents a very small fraction (3%) of the soil size distribution. Moreover, the roughness length derived from POLDER-1 in the Taklimakan desert is lower than in the other sandy deserts and is often below 10^{-2} mm. Therefore, the smooth roughness length for the Taklimakan desert is derived as 1/30 of the finest mass median diameter (Table 2).

It should be noted that the simulations are very sensitive to this parameter in some specific regions. In the Taklimakan desert, due to the low value of the POLDER-1 derived roughness length, shifting the smooth roughness length from 10^{-2} to 10^{-3} mm can transform a smooth erodible surface in a relatively rough and thus less erodible surface. On the contrary, in the gobi desert of Mongolia, due to high POLDER-1 derived roughness length, shifting the smooth roughness length from 10^{-3} to 10^{-2} mm can transform a non erodible surface into an occasional source of very intense dust events.

3.1.2.3. Chinese soil texture. In addition to the "dry" soil size distribution, Mei et al. (2004) measured the soil texture of their individual samples except those of the Horqin sandy land (Table 1). The median clay contents of are always low (<12%), especially in the sandy deserts (Ulan Buh, Mu Us, Taklimakan and Tengger) where it never exceeds 3.4% (with a S.D.<1.4%). Both the median and standard deviation of the clay content are higher (up to 9.9% clay and S.D.~6% to 7%) in the other desert areas (Gurban Tunggut, East of Xinjiang and Hexi Corridor). The samples from Inner Mongolia exhibit the highest median clay content (11.9%), but with a relatively low standard deviation (3.9%).

For the individual soil samples, the soil clay content does not show any co-variation with the statistical parameters of the soil size distribution (MMD_i or P_i). The only trends that can be drawn from Fig. 3a,b are (1) that high silt and clay contents (clay >10% and silt >30%) are often associated to low MMD_1 (60 to 100 μm) and (2) that the highest values of MMD_1 (100–200 μm) are associated with high sand content (>80%). However, these trends are not exclusive: a coarse MMD_1 is not a systematic feature of soils with low clay content and, similarly, a low MMD_1 is not systematically associated with high clay content. These results point out the fact that there is no systematic relationship between soil textures and soil dry size distributions.

The range of median soil clay content measured for Chinese soils is comparable to the ones measured in northern America arid soils (Gillette, 1979) or estimated over the Sahara (Marticorena et al., 1997a). As a result, they may have a comparable efficiency in producing dust.

The texture of the Horqin sandy land samples was not measured. The Horqin sandy land is geographically close to the Mu Us sandy land and these two areas are both partly vegetated with semi-fixed dunes (Walker, 1986; Mainguet, 1996). The soil size distributions derived for the Horqin sandy land and the Mu Us desert are comparable. As a result, the soil clay content for the Horqin sandy land was considered equal to the soil clay content of the Mu Us desert. The same soil clay content was also assigned to the Hulun Buir and the Otin Daq sandy lands.

To estimate the soil clay content of the loess and sandy loess, we used the soil texture determined by Ding et al. (1999) for soil samples collected in the northwestern part of the Loess Plateau in Xinzhuangyuan (sandy loess) and in Lijiayuan (loess). For both regions, the clay content of the first 20 mm of soil ranges from 15% to 18%. A typical value of 17% was therefore used as representative of the loess and sandy loess clay content.

3.1.2.4. Residual soil moisture and ratio of vertical to horizontal flux. For each documented area, the clay content is used to estimate the residual soil moisture w' (Eq. (5)) and the ratio of vertical to horizontal flux α (Eq. (7)), as summarized in Table 2. Over the various arid and semi-arid areas of eastern Asia, the range of α covers 3 orders of magnitude. In the desert areas, it varies from 1.64×10^{-7} mm^{-1} in sandy areas up to 3.93×10^{-6} mm^{-1} for the gobi surface. They are in the same order of magnitude than the ones measured by Gillette (1979). Due to high clay content, a maximum of 1.90×10^{-5} mm^{-1} is estimated in the loess and sandy loess areas.

3.1.3. Fraction of erodible surface, E

The dust flux computation also requires the fraction of erodible surface E (Eq. (6)). This parameter, which has a linear effect on the dust emission flux, corresponds to the part of the surface, which is not protected from wind erosion by roughness elements.

The only information we have for the Chinese and Mongolian deserts in terms of surface features are the roughness length Z_0, derived from POLDER-1. Marticorena et al. (1997a) have established an empirical relationship between Z_0/h and the roughness density λ, h being defined as the mean height of the roughness elements. The roughness density is defined as:

$$\lambda = \frac{nbh}{S} \tag{8}$$

where n is the number of roughness elements of height h and width b over a surface S.

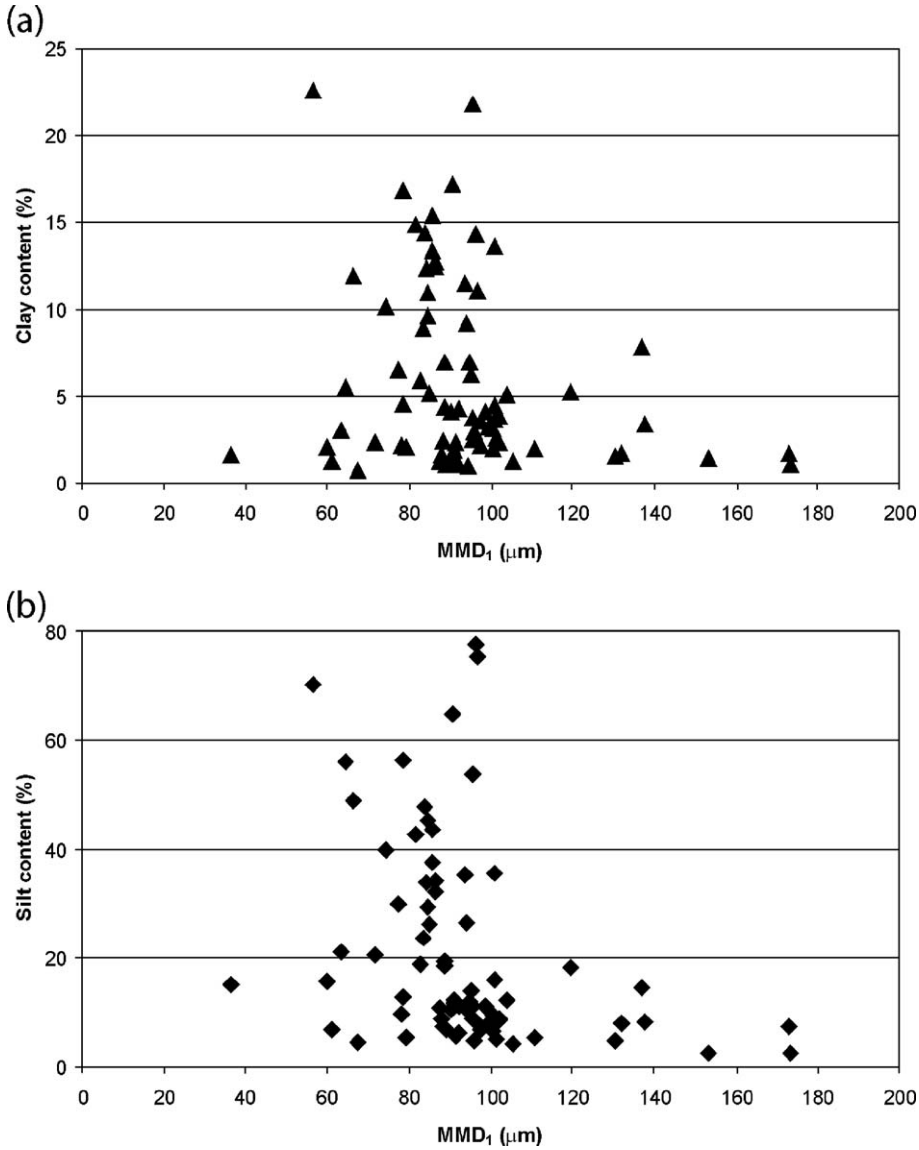

Fig. 3. Clay (a) and silt (b) contents as a function of the mass median diameter MMD_1 of the finer mode of the soil size distribution for individual samples collected in the main desert areas of China (data from Mei et al., 2004).

Thus, it should be possible to derive the covering rate of the roughness elements, i.e., $(1-E)$ from the roughness length with additional hypothesis on the obstacle shapes. For example, assuming cubic obstacles ($h=b$), the roughness density is equivalent to the covering rate of the obstacles. However, as mentioned above, λ is linearly linked to Z_0/h and not to Z_0.

For natural surfaces where various types of gravel, pebbles, etc. of various shapes and dimensions can co-exist over the same surface, the assessment of the roughness density or covering rate of roughness elements based on the roughness length Z_0 requires to estimate the equivalent mean height of the obstacles.

We used the data set of surface features established by Callot et al. (2000) over the Sahara desert. This data set is based on a geomorphological mapping of the characteristics of the roughness elements: mean height and covering rates for the gravel, pebbles and other non-erodible elements present on the surface.

From this data set, we computed the median covering rates for logarithmic classes of roughness length (Fig. 4). The fraction of erodible surface clearly decreases as a function of the roughness length, but with a significant

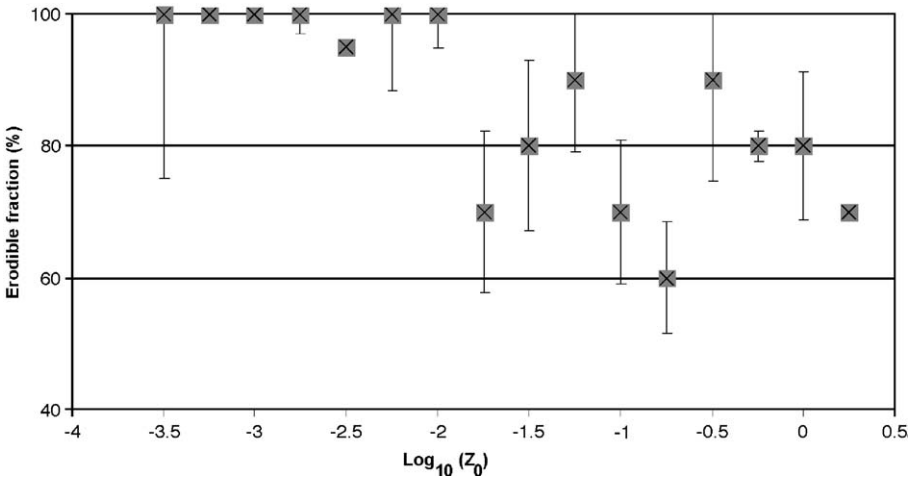

Fig. 4. Relationship between the fraction of erodible surface E and the aerodynamic roughness length estimated over the Sahara and the Arabian Peninsula (based on the data from Callot et al., 2000).

dispersion. This is consistent with the relationship between λ and Z_0/h, which suggests as many different linear relations as there are different heights or shapes for the roughness elements. It must be noted, however, that the dispersion associated to each median value is relatively low (<25%).

We thus decided to use only one linear relationship between E and Z_0. The correlation coefficient associated with this linear fit for erodible fractions smaller than 100% ($Z_0 > 3 \times 10^{-2}$ mm) is not very high, but the differences between the erodible fraction computed with this relationship and the median values from Callot et al. (2000) are always lower than 30%. This relationship was thus applied to estimate E over the surfaces where $Z_0 > 3 \times 10^{-2}$ mm.

3.2. Parameters relative to the meteorological conditions

The meteorological parameters used for this study are extracted from the ERA-40 database of the European Center for Medium-range Weather Forecast (ECMWF). The ECMWF Re-Analysis (ERA-40) project has produced a comprehensive global analysis for a 45-yr period ending in 2002, making optimal use of a wide range of observing systems (Betts and Beljaars, 2003), especially satellite observations. A recent version of the ECMWF Numerical Weather Prediction system was used for the entire analysis period (Uppala et al., 2004). As a result, the ERA-40 analyses had shown considerable success in reproducing realistic trends over the last four decades. The comparisons of the ERA-40 near surface data with selected surface observations (surface temperature, dew point, precipitation, etc.) also indicates that ERA-40 has a realistic representation of the seasonal anomaly fields on a global scale (Betts and Beljaars, 2003).

The meteorological surface parameters used for the computation of dust emission fluxes are the surface wind velocities, the snow cover and the soil moisture which is computed using the daily precipitation and minimum and maximum air temperature, the albedo and the geopotential. All the meteorological parameters are re-analyzed data products except the precipitation that are re-forecasted data.

3.2.1. Surface wind velocity

To compute the wind shear stress, we used the ERA-40 surface wind fields at the spatial resolution of 1/4° × 1/4° from 1996 to 2001. The surface wind fields are instantaneous values of the two horizontal components u and v of the horizontal wind which are defined at 10 m height, for 00h00, 06h00, 12h00 and 18h00 UT. The wind velocity norm $(u^2+v^2)^{1/2}$ has been computed from u and v to obtain a 10-m wind velocity field.

Laurent et al. (2005) used the operational analysis archive (OAA) from ECMWF and noticed some bias in the surface wind velocity fields compared to those measured in the meteorological stations or during specific dust events. They noticed that the frequency of wind velocity higher than 6.5 m s^{-1} derived from OAA were lower than the observed, in particular in the northern deserts of China and in Mongolia. We thus compared the ERA-40 surface wind field to those used by Laurent et al. (2005) for the years 1997 to 1999. For example, in 1997, the surface velocity

from the two data sets are highly correlated (r=0.79, n (number of data)=1005,940, slope=0.81). The ERA-40 surface wind velocities are generally slightly higher than the OAAs, especially in the range of low wind velocities. On the contrary, the maximum wind velocities are larger. Indeed, over the Gobi desert of Mongolia and Inner Mongolia (China), the ERA-40 surface wind velocities never exceed 12 m s^{-1}, while a few values exceed 15 m s^{-1} in the OAA. The main difference between the two data sets is the spatial pattern and the intensity of the frequencies of wind velocity higher than 6.5 m s^{-1}. Over the northern deserts of China and the Gobi desert, the frequencies of wind velocity higher than 6.5 m s^{-1} are locally comparable for the two data sets, but the area for which this threshold velocity is exceeded is much wider for the ERA-40 database than for the OAA one. On the contrary, in the Taklimakan desert, the frequencies of wind velocity higher than 6.5 m s^{-1} are lower in the ERA-40 database but the area for which the wind velocity is higher than 6.5 m s^{-1} is similar in the two data sets.

3.2.2. Soil moisture

The dust emission model includes the parameterization of the soil moisture influence on the erosion threshold proposed by Fécan et al. (1999). The gravimetric soil moisture, w, is used as an input parameter.

Soil moisture fields are among the reanalysis products available in the ERA-40 database. They are computed based on the land surface scheme using four prognostic soil layers (Van Den Hurk et al., 2000). However, the soil physical treatment is uniform since a unique homogeneous loamy texture is used in the four layers and over the whole land surface. As a result, this model does not reproduce well the very low soil moisture contents measured in semi-arid areas such as the Sahel, that are mainly characterized by sandy soils (Van Den Hurk et al., 2000).

In this study, the soil moisture content has been computed, like in Laurent et al. (2005), based on a water balance model (Mougin et al., 1995) and using up to 14 soil layer as specified in the texture profiles (Webb et al., 2000) associated to the global FAO soil texture map (Zobler, 1986). The texture of the superficial layer (20 mm) is derived from the analysis of in-situ sampling (Ding et al., 1999; Mei et al., 2004).

3.2.3. Snow cover

Following Laurent et al. (2005), we assume that snow cover (i.e., snow depth > 0) inhibits dust emission by totally protecting the erodible surface from erosion. To account for the snow cover, we used the ERA-40 daily snow depth at the resolution of 1/4° × 1/4°.

4. Simulations of mineral dust emission

Mineral dust emissions over the Chinese and Gobi deserts are estimated based on the previous input data. The erosion thresholds (U_t^*) are computed for each grid mesh with a daily time step based on the POLDER-1 derived roughness length (Z_0), the estimated smooth roughness length (z_{0s}) and the soil moisture. If the surface wind velocity exceeds the erosion threshold and if snow depth is equal to 0, an instantaneous dust flux is computed in each grid mesh with a 6-h time step from the surface wind velocity, the soil size distribution and the ratio of vertical to horizontal flux (α). The daily fluxes are estimated assuming that the instantaneous fluxes are representative of a 6-h interval. The daily fluxes (in g cm^{-2} day^{-1}) are weighted by the grid mesh surface to obtain dust emission amount (g day^{-1}) for each 1/4° × 1/4°.

The results are discussed in terms of individual dust events, seasonal cycle, annual dust emissions and inter-annual variability and compared with observations and/or data from the literature. It can be noticed that very few direct observations and no direct measurements of the dust emissions are available.

4.1. Simulation of individual dust events

To test the relevance of the dust emission simulations, we first focused on specific dust events occurring over short periods of time. The two selected periods (April 1998 and spring 2001) correspond to dust events well documented both by the meteorological stations, by the SeaWiFS, TOMS and AVHRR space sensors, and by sun photometers from the AERONET network (Husar et al., 2001; Zhang et al., 2003). During these periods, only few events of short duration occurred but the dust amount emitted during each event was generally very large. For example, in April 1998, dust events have lead to surface aerosol concentrations two to four times higher than for any other dust event since 1988 (Husar et al., 2001). These dust events have been interpreted by an ad hoc international web-based virtual community (Husar et al., 2001) and as a part of the ACE-ASIA international program. As a result, this information can be used in terms of (1) occurrence, (2) location of the dust source and (3) relative intensity of the dust events.

To further validate the simulations of individual dust events, we compared the simulated dust

emissions to the reductions of horizontal visibility recorded by the meteorological stations. Indeed, in arid and semi-arid areas, a horizontal visibility below 1000 m, is generally due to a dust storm (Middleton, 1989). However, such a low visibility can also be associated to the presence of fog. Thus, the number of dust storms estimated from the reduction of the horizontal visibility may be overestimated, especially in the northern and eastern part of the simulated area. To minimize this bias, we selected the meteorological stations close to the mineral dust sources: 14 stations for the Taklimakan desert, 23 stations for the northern deserts of China, i.e., the Badain Jaran, Ulan Buh, Tengger, Qubqi and Mu Us deserts and 20 stations for the Gobi desert. In the following, a "dust storm" record will be defined as a horizontal visibility below 1000 m recorded at least once a day in a meteorological station. Depending on the meteorological station, the visibility is reported with a 3- or 6-h time step.

4.1.1. April 1998

The daily simulated dust emissions (a) and the number of meteorological stations that recorded a dust storm (b) are reported on Figs. 5 and 6, respectively, for the Taklimakan desert, and for an area including the northern deserts of China and the Gobi desert. Figs. 5 and 6 show that the periods when the most intense dust emissions are simulated correspond to the periods when the number of stations recording dust storms is the highest.

The agreement score between the simulation and the observation is of 70% for both the Taklimakan desert, and the Gobi and northern deserts (Table 3). For some cases, dust storms are observed by the meteorological stations 1 day after dust emissions are simulated. This delay can be partly explained by the relatively large distances separating the meteorological stations from the dust emission sources. The number of dust storm days is similar in the Taklimakan desert and in the area of the Gobi and northern deserts. However, in the latter,

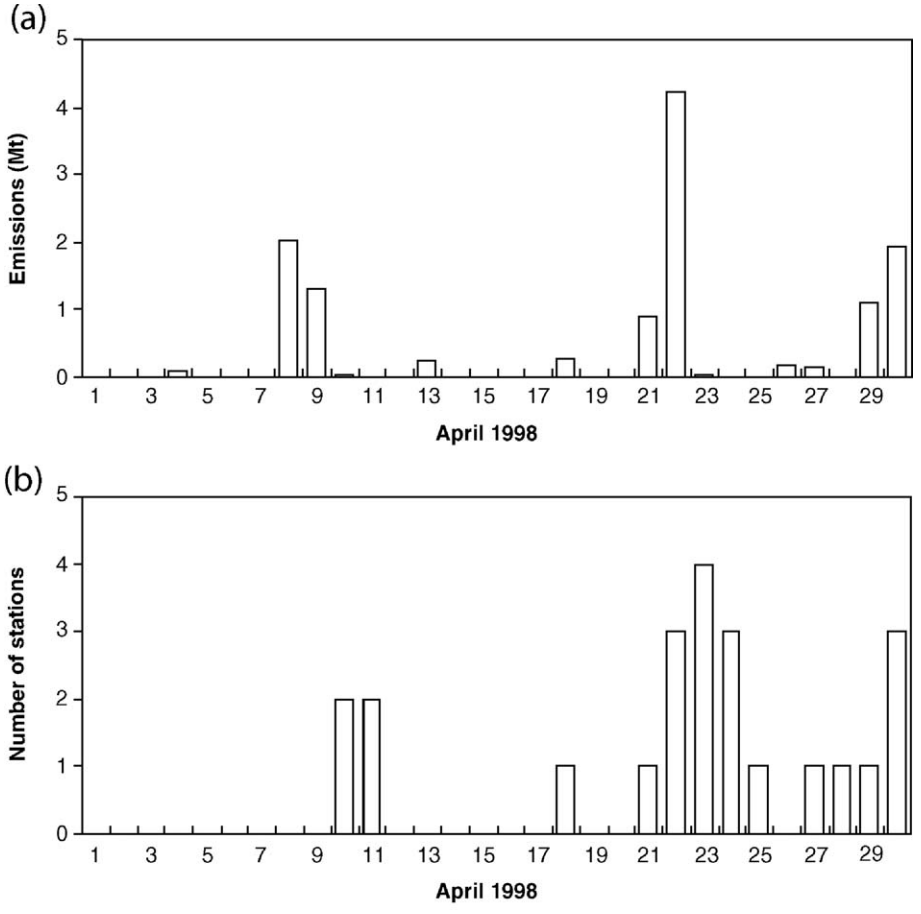

Fig. 5. Daily simulated emissions (a) and daily number of stations that observed a dust storm (b) in April 1998 in the Taklimakan desert area.

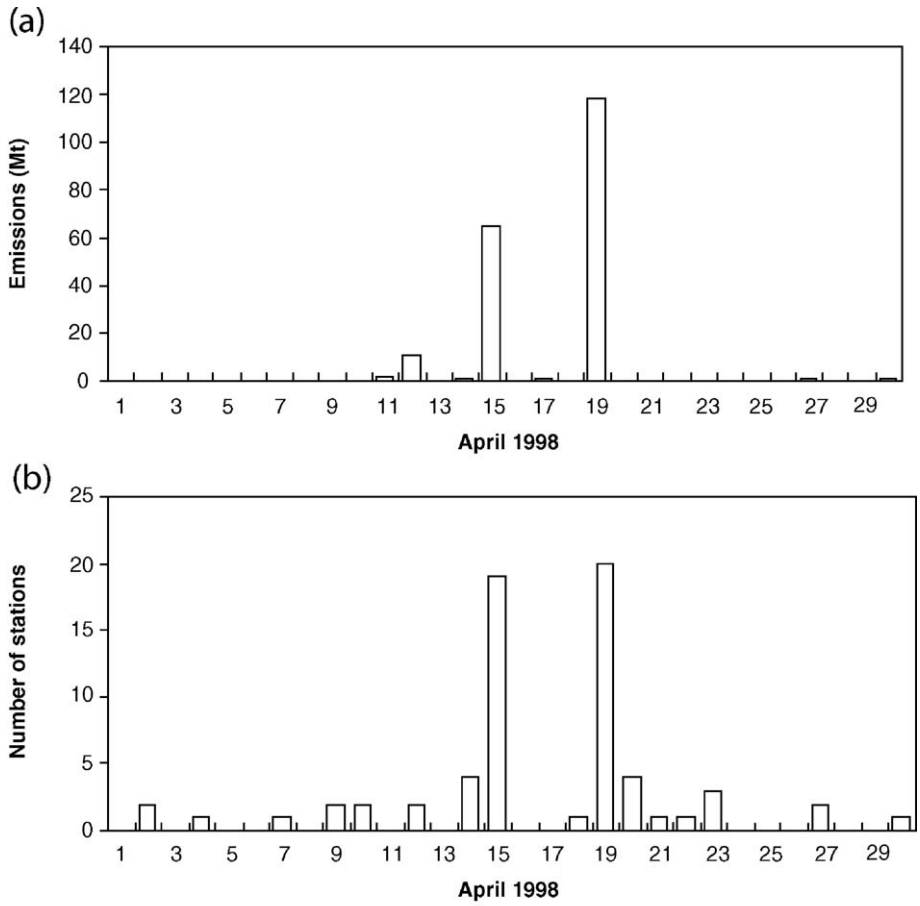

Fig. 6. Daily simulated emissions (a) and daily number of stations that observed a dust storm (b) in April 1998 in the northern deserts of China and in the Gobi desert.

the simulated dust emissions are higher, mainly due to the two huge events on April 15 and 19.

On April 15, 19 out of the 43 stations located in the northern deserts and Gobi desert areas recorded dust storms. On April 19, the phenomenon was slightly more pronounced with 20 out of the 43 stations. Based on the in situ measurements (horizontal visibility, daily PM10 concentrations) and remote sensing (TOMS aerosol Index, SeaWIFS images), Husar et al. (2001) suggest that the April 19 dust storm was the more intense event, causing the highest regional average dust concentrations. Our simulations are consistent with this statement since the simulated dust emissions are 65 Mt for April 15 and 118 Mt for April 19.

Table 3
Number of days of daily agreement and disagreement between the simulated dust emissions and the observed dust storm in April 1998 (30 days) and spring 2001 (92 days) in the Taklimakan desert (TK) (35.5°N–42°N, 75°E–90°E), the northern deserts of China (ND) (37°N–42°N, 99°E–111°E) and the Gobi desert (GB) (42°N–46.5°N, 90°E–115°E)

Period	Area location	Agreement (in days)		Dust event simulated and observed the day after (in days)	Disagreement (in days)	
		Dust event	No dust event		Dust event simulated	Dust event observed
April 1998	TK	9	12	6	3	–
	ND and GB	11	10	4	2	3
Spring 2001	TK	22	40	9	12	9
	ND and GB	39	31	5	15	2

In terms of dust source location, it can be noted that the April 15 dust storm was recorded by meteorological stations located both in northern deserts and in the Gobi desert of Mongolia, whereas the April 19 dust storm was mainly recorded by the meteorological stations located in the vicinity, or inside, the Gobi desert area. According to our simulations, for April 15, most of the dust (65%) was emitted from the northern deserts of China and 35% from the Gobi desert. On the contrary, on April 19, the simulations point out the Gobi desert as the main source with more than 97% of the simulated emissions originating from this area.

As a conclusion, the dust emission occurrence, the different dust source locations in time and space, and the relative intensity of the different dust events during April 1998 are well simulated. Our simulations are in agreement with the visibility below 1000 m recorded by the meteorological stations and with the previous studies performed on the main dust storms originating from the northern deserts of China and the Gobi desert at this period (Husar et al., 2001).

4.1.2. Spring 2001

A similar comparison was carried out for the period extending from March to May 2001 (Figs. 7 and 8). Like for April 1998, the simulated occurrence of dust emissions and the recorded dust storm days are in good agreement. The number of dust storms recorded in the area of the northern desert of China and in the Gobi desert is comparable to the one recorded in the Taklimakan desert. However, especially during March and May 2001, many very low dust events are simulated which are not always observed by the meteorological stations. April appears as the month of spring 2001 with the most intense dust emissions.

Globally, the simulated emissions and the recorded visibility below 1000 m are in good agreement. In the Taklimakan desert, the agreement is 67% and even higher (76%) in the Gobi and northern deserts (Table 3).

Both the simulations and the recorded visibility point out the Gobi and northern deserts as the major dust sources. Two huge events, occurring on April 6 and April 29, have been recorded by meteorological stations located inside or close to the northern deserts of China

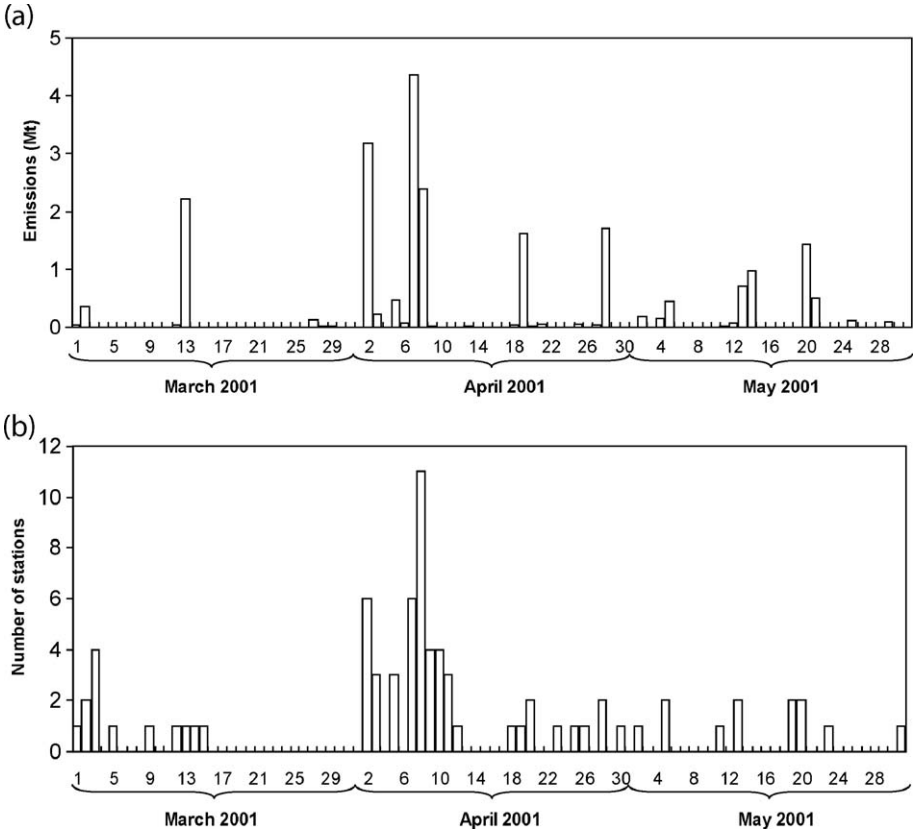

Fig. 7. Daily simulated emissions (a) and daily number of stations that observed a dust storm (b) in spring 2001 in the Taklimakan desert area.

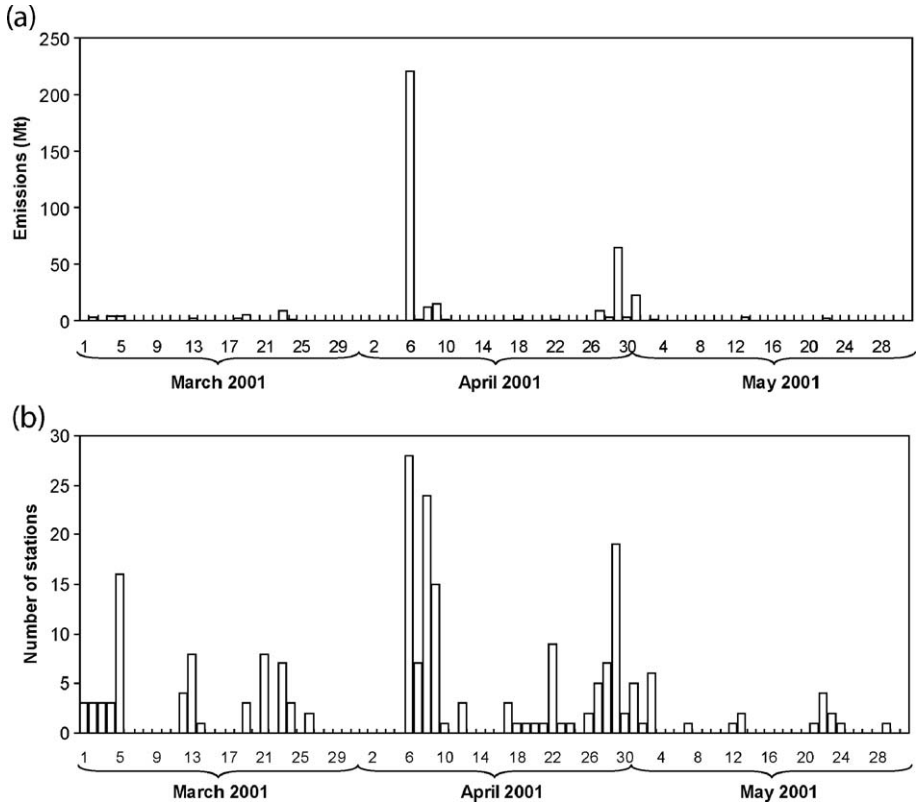

Fig. 8. Daily simulated emissions (a) and daily number of stations that observed a dust storm (b) in spring 2001 in the northern deserts of China and in the Gobi desert.

and Gobi desert. On April 6, 28 out of the 43 stations located in the area of the Gobi and northern deserts recorded dust storms, but only 18 on April 29.

For the spring 2001, Gong et al. (2003) identified the dust storm event occurring between April 4 and 14 as the most intense and persistent, since they simulated 66 Mt of emitted dust. A second major dust storm is simulated from April 29 to May 5 with 51 Mt of emitted dust. In our simulation, 221 Mt are emitted during the April 6 dust storm. A second, less severe, dust storm is simulated on April 29 with 65 Mt of emitted dust. Our simulations are consistent with the study of Gong et al. (2003) in terms of period and relative intensity of the two dust events. However, for the whole period between April 4 and 14, our simulations suggest much higher emissions (250 Mt) than Gong et al. (2003). For the second event (April 29 to May 5), the difference with Gong et al.'s (2003) simulations is less than a factor of 2. For the whole spring 2001, the total dust emission is estimated to about 253 Mt by Gong et al. (2003), whereas our total dust emission is 40% higher, i.e., 418 Mt.

Using a high resolution regional dust model, Liu et al. (2003) also estimated the dust emissions (of particles smaller than 10 μm in diameter) between April 5 and April 15 to 550 Mt.

We can conclude that our simulated dust emissions are comparable to those obtained by other models and suggest that the uncertainty on the dust emissions from Asian sources is at least of the order of 50%.

4.2. Major sources of dust emissions

We have computed the annual dust emissions (Fig. 9a) and the number of dust events (Fig. 9b) averaged over the 6-yr simulated period (1996–2001). The number of dust events corresponds to the number of time the erosion threshold is exceeded, i.e., a dust emission is simulated.

About 98% of the annual dust emissions originate from three main desert areas: the Taklimakan desert, the northern deserts of China and the Gobi desert. These three areas have a comparable contribution to the total dust emissions, respectively, 27%, 33% and 38%. On the contrary, their contributions to the total number of dust events are radically different: 59% for the Taklimakan desert, 37% for the northern deserts of

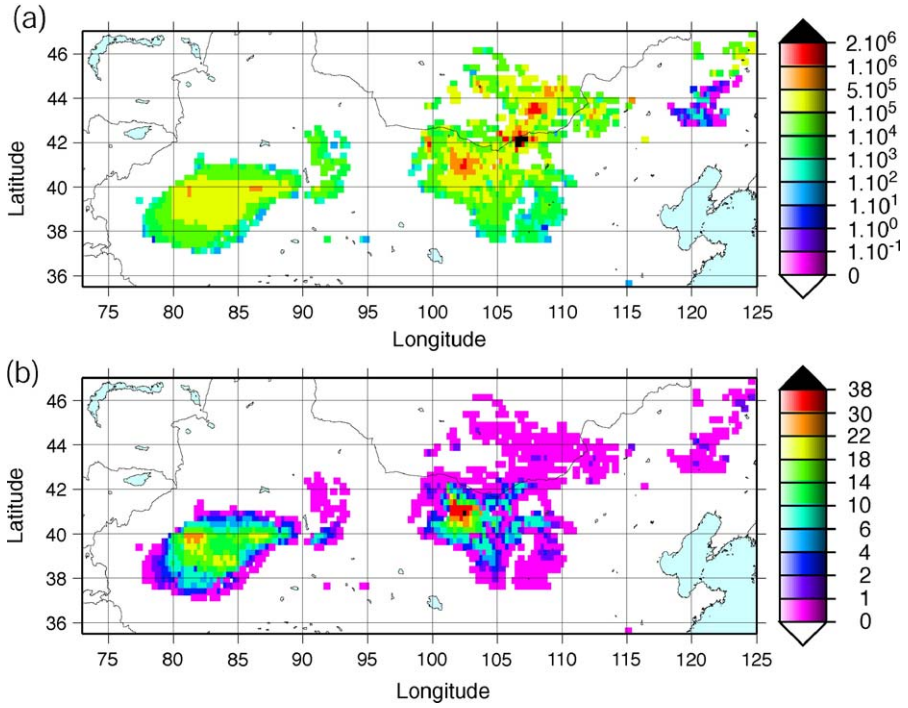

Fig. 9. Annual dust emissions averaged (in t yr^{-1}) over the period 1996–2001 (a); annual number of dust event days averaged over the period 1996–2001 (b).

China and only 2% for the Gobi desert. The main contribution of the Taklimakan desert to the total number of dust emission events is due to the fact that the erosion thresholds, generally low, are frequently exceeded over a large area. On the contrary, in the Gobi desert, the presence of gravels and pebbles leads to high threshold wind friction velocities and, as a consequence, very few dust emissions events are simulated. However, when the threshold is exceeded, because of the very high wind velocities, the dust events are generally huge events. The annual dust emissions can reach more than 2 Mt yr^{-1} per $1/4° \times 1/4°$ surfaces in this area. The northern deserts of China exhibit an intermediate behaviour: the number of dust events is locally higher than in the Taklimakan desert and annual dust emissions for some $1/4° \times 1/4°$ surfaces are comparable to the highest emissions simulated in the Gobi desert. Only 2% of the annual dust emissions come from other regions than these three main areas. Most of these emissions are produced over the Horqin sandy land, suggesting that this area could be an episodic but significant dust source.

Laurent et al. (2005) simulated the dust emissions frequencies over the Chinese and Mongolian deserts from 1997 to 1999. They identified the Taklimakan and the northern deserts of China as the most frequent dust sources, with the highest dust event frequency in the northeastern part of the Taklimakan desert. However, they noted that the dust emissions frequencies over the deserts of northern China and Gobi desert were underestimated compared to the dust storm frequencies derived from synoptic observations. It is mainly due to a bias in the ECMWF OAA surface wind fields. The use of the ERA-40 surface wind fields tends to give more weight to these areas in the total dust emission frequencies, and thus a better agreement with the observed dust storm frequencies (Sun et al., 2001; Natsagdorj et al., 2003) is obtained. The highest dust emission occurrence is simulated in the northern deserts of China, more precisely in the Badain Jaran desert, in agreement with the analyses of the dust storm frequencies in Inner Mongolia (Gao et al., 2003). However, due to a larger extend, the Taklimakan desert remains the region where the highest number of dust emission events is simulated.

Zhang et al. (2003) simulated the dust emissions from Asian arid and semi-arid areas for the period from 1960 to 2002. As a comparison, the relative contribution of the three main desert areas defined by these authors are respectively 21% (±7) in the Taklimakan desert, 26% (±8) in the northern deserts of China (Badain Jaran, Tengger, Ulan Buh, Mu Us and Qubqi deserts) and 29%

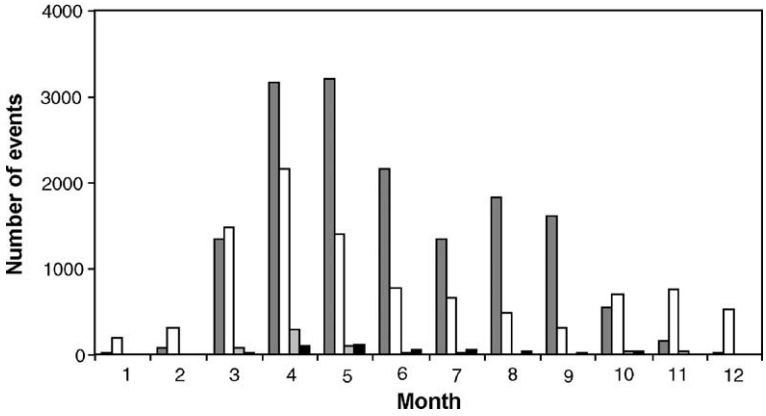

Fig. 10. Seasonal variations of the monthly number of dust events simulated with a 6-h time step for the Taklimakan desert (dark grey), the northern deserts of China (white), the Gobi desert (light grey) and the other arid areas (black) averaged over the period 1996–2001.

(±10) in the Gobi desert of Mongolia. Our results are thus consistent with these long-term simulations.

4.3. Seasonal cycle

The seasonal cycle derived from synoptic observations is clearly characterized by a maximum in spring with some minor differences depending on the region (Sun et al., 2001; Gao et al., 2003; Natsagdorj et al., 2003; Sun et al., 2003; Wang et al., 2003). For example, a secondary maximum in the dust storm frequencies can be observed during winter (December and January) in the northern deserts of China and during the fall in some stations of Mongolia or Inner Mongolia (Gao et al., 2003; Natsagdorj et al., 2003; Sun et al., 2003). The period of maximum dust storm frequencies in the Taklimakan desert extend from spring to early summer (Sun et al., 2003; Wang et al., 2003).

The simulated occurrence of dust events also exhibits a period of maximum from spring to early summer in the Taklimakan desert and a secondary maximum during winter in the northern deserts of China (Fig. 10). The seasonal cycle of the dust emissions shows the same general trends as the dust emission frequencies but with higher seasonal and spatial contrasts (Fig. 11). The spring is clearly the dustiest season in China and Mongolia. For example, 79% of the annual emissions from the Gobi desert occur in April. The dust emissions are also maximum in spring (April) in the northern deserts of China and in the Horqin sandy land and between April and May in the Taklamakan. Due to a secondary maximum between August and September, the Taklimakan desert is the main dust source area during late summer and early fall. The emissions from the other arid areas mainly originate from the Horqin sandy land. They exhibit a secondary peak in November (1.4 Mt to be compared to 1.9 Mt in the spring). In

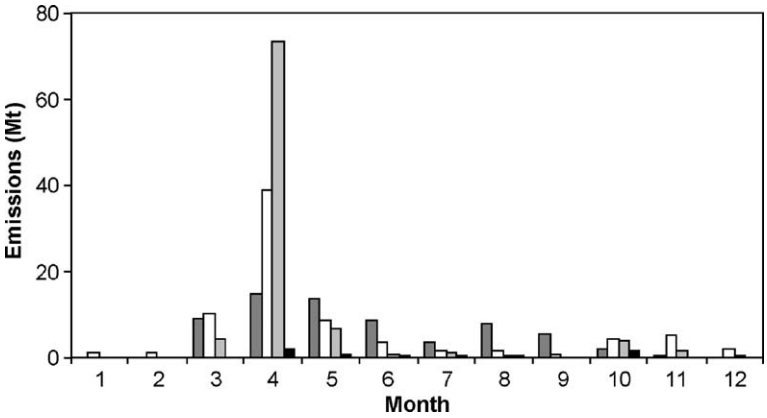

Fig. 11. Seasonal variations of the monthly dust emissions for the Taklimakan desert (dark grey), the northern deserts of China (white), the Gobi desert (light grey) and the other arid areas (black) averaged over the period 1996–2001.

Table 4
Annual emissions from 1996 to 2001 for the whole studied area (total), the Taklimakan desert (TK), the northern deserts of China (ND), the Gobi desert (GB) and the other arid areas of China and Mongolia (other)

	Mineral dust emissions (10^6 t)				
	TK	ND	GB	Other	Total
1996	94	72	26	12	204
1997	68	19	10	4	100
1998	80	99	149	3	332
1999	62	59	27	4	151
2000	46	96	61	2	205
2001	41	126	285	7	459
Mean	65	79	93	5	242
σ	20	37	107	4	131

winter, the northern deserts of China are the major dust source over the simulated area.

4.4. Inter-annual variability

4.4.1. Annual dust emissions

The average annual dust emissions from Chinese and Mongolian deserts over the 6 yr of simulations is 242 Mt, but the annual dust emissions vary from 100 Mt in 1997 to 459 Mt in 2001 (Table 4), underlining a high inter-annual variability.

The Taklimakan desert appears as a steady dust source over the 6 simulated years. The inter-annual variability of the simulated dust emissions is only of a factor 2, with a maximum in 1996 and a minimum in 2001. It reaches a factor 6 in the northern deserts of China and a factor 28 in the Gobi deserts. In both regions, the minimum dust emissions among the 6 yr are simulated for 1997, while 1998 and 2001 are characterized by very intense dust activity.

Based on dust deposition measurements in the main desert and deposition areas of China, Zhang et al. (1997) estimated the total dust production from Chinese deserts to ~800 Mt yr^{-1} with an estimated range from 500 Mt yr^{-1} to 1100 Mt yr^{-1}. Our estimation of 100–460 Mt yr^{-1} is significantly lower. However, it only corresponds to the emissions of dust particles having a diameter smaller than 20 μm, while dust deposition in the vicinity of source regions is significantly affected by coarser particles. For the spring, the 6-yr averaged simulated dust emissions (182 Mt) are comparable with the 43-yr averaged dust emissions (120 Mt) simulated by Zhao et al. (2004). The most recent dust budgets estimated at a global scale range from 1000 Mt yr^{-1} to 2150 Mt yr^{-1} (Zender et al., 2004). With annual dust emissions of the order of 240 Mt, our simulations suggest that Asian deserts could represent between 10% and 25% of the annual mineral dust emissions at the global scale.

4.4.2. Causes of the inter-annual variability of dust emissions

Over the 6-yr simulation, the inter-annual variability of the dust emissions is mainly related to changes in the intensity of the spring dust emissions (Fig. 12). On the contrary, the total number of dust emission events exhibits a regular pattern over the 6 yr (Fig. 13). As discussed in Section 4.1, the extremely high dust emissions in April 1998 and 2001 are related to the

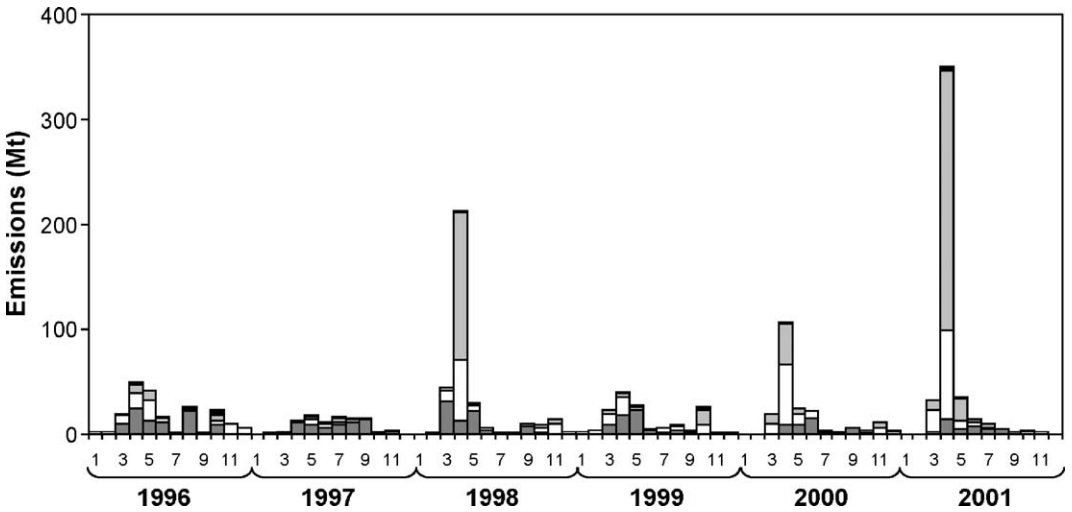

Fig. 12. Monthly dust emissions simulated for the Taklimakan desert (dark grey), the northern deserts of China (white), the Gobi desert (light grey) and the other arid areas (black) from January 1996 to December 2001.

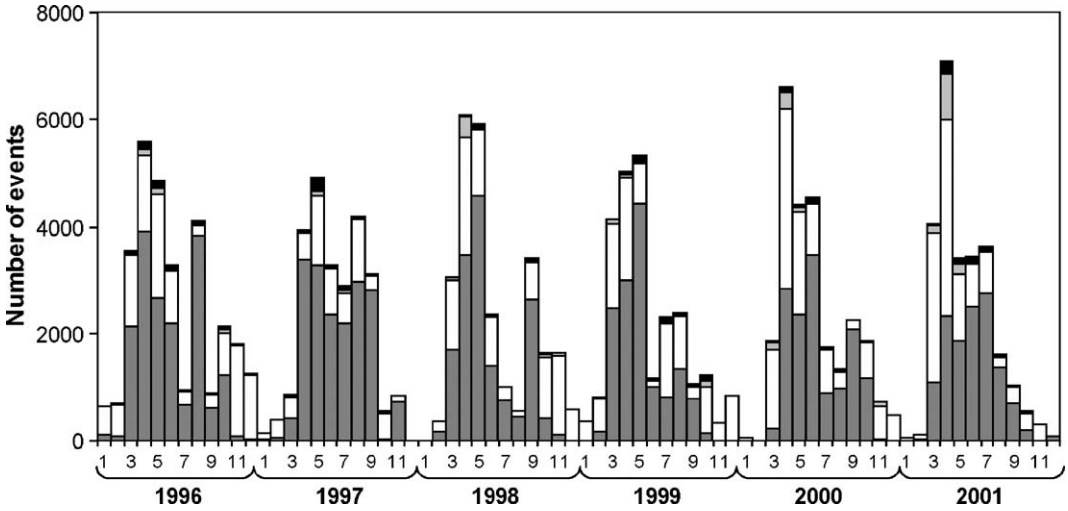

Fig. 13. Monthly number of dust events simulated with a 6-h time step for the Taklimakan desert (dark grey), the northern deserts of China (white), the Gobi desert (light grey) and the other arid areas (black) from January 1996 to December 2001.

occurrence of few unusually intense dust storms. These huge dust events mainly originate from the northern deserts of China and from the Gobi desert.

The regular pattern of the number of dust emission events is mainly driven by the dust emissions from the Taklimakan desert. However, a significant increase in the occurrence of the dust emissions from the northern deserts of China and the Gobi desert is simulated for spring 2000 and 2001. The simulations suggest that the inter-annual variability of the dust emissions in China and Mongolia is mainly driven by the sudden occurrence of extremely high wind velocities over the desert areas exhibiting the highest erosion thresholds. They also suggest a trend of increase in the occurrence of dust emissions in the northern deserts of China and in the Gobi deserts, in agreement with the observations (Kurosaki and Mikami, 2003).

4.4.3. Influence of soil moisture and snow cover

Soil moisture and snow cover affect the dust emissions. However, Laurent et al. (2005) showed that these effects on dust event frequencies are very limited. Our simulations give the opportunity to examine their impact on dust emissions. We performed simulations without accounting for the effects of the soil moisture and snow cover. These simulations were compared to the results previously presented and the differences between the two simulations are discussed.

The general pattern of the seasonal cycle of dust emissions is not significantly influenced by the soil moisture and the snow cover (Table 5). During the most intense period of dust emissions (March, April and May), the influence of the soil moisture and snow cover is relatively weak (respectively, 7%, 5.5% and 4%). However, accounting for the influence of the soil moisture and snow cover decreases respectively by 94% and 84% the dust emissions in January and December. This suggests that soil moisture and snow cover control the dust emissions in winter.

Due to low precipitation and snow falls, the dust emissions of the Taklimakan desert are not noticeably influenced by the soil moisture and the snow cover. On the contrary, they significantly limit dust emissions in

Table 5
Decrease in the simulated monthly dust emissions during the period 1996–2001 due to the influence of the soil moisture and snow cover for the whole studied area (total), the Taklimakan desert (TK), the northern deserts of China (ND), the Gobi desert (GB) and the other arid areas of China and Mongolia (other)

	Relative decrease in dust emissions due to soil moisture and snow cover (%)				
	TK	ND	GB	Other	Total
January	1.1	80.2	99.9	100.0	94.2
February	10.5	44.1	95.5	100.0	68.0
March	3.0	3.3	16.8	80.0	7.1
April	7.4	4.7	3.6	46.7	5.5
May	1.8	3.3	3.6	34.9	3.9
June	0.1	2.2	10.9	26.6	1.9
July	1.3	3.9	2.1	9.4	2.4
August	0.7	11.2	11.7	42.9	5.9
September	0.1	0.5	8.2	20.5	0.7
October	3.1	16.2	33.0	35.4	23.8
November	40.2	18.4	35.3	13.4	24.7
December	55.5	73.2	96.7	100.0	83.9

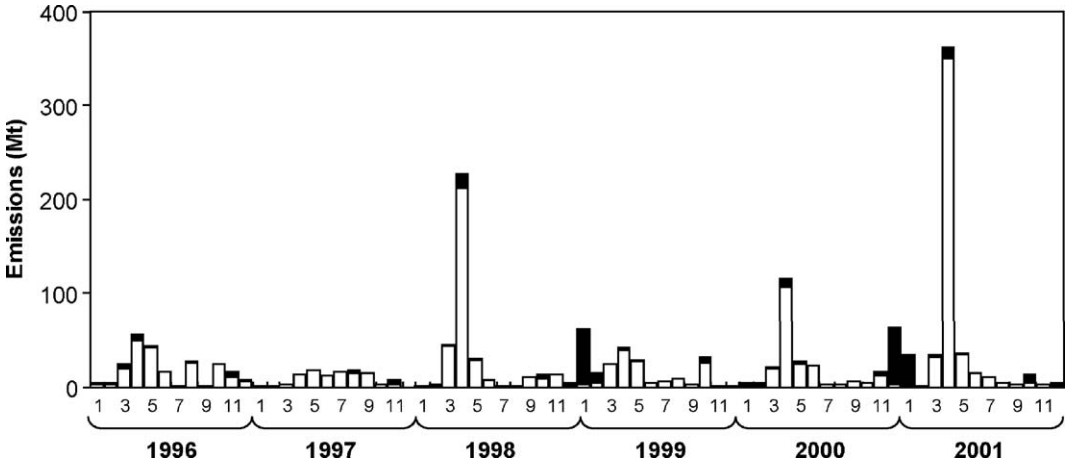

Fig. 14. Monthly dust emissions simulated from January 1996 to December 2001 with (white) and without (black) accounting for the influence of soil moisture and snow cover on the dust emissions.

the northern deserts of China, the Gobi desert and the Horqin sandy land.

The inter-annual variability of the dust emissions is not significantly influenced by the soil moisture and snow cover (Fig. 14), since it is mainly controlled by spring dust emissions events. However, soil moisture and snow cover reduce the winter dust emissions to less than 5 Mt, while they can reach 60 Mt when these two factors are neglected.

5. Conclusion

Mineral dust emissions have been simulated over the period 1996–2001 to provide a quantitative estimation over Chinese and Mongolian arid and semi-arid areas. Special attention was given to the production of relevant input parameters data sets: the roughness lengths were derived from the bi-directional reflectance distribution functions from the space-borne POLDER-1 sensor, a specific database for soil size distributions and textures was derived from in-situ measurements (Ding et al., 1999; Yang et al., 2001; Mei et al., 2004) and meteorological data from the ECMWF ERA-40 database were selected.

The simulations reproduce well, on a daily basis, of the huge dust events that occurred in April 1998 and spring 2001 in terms of timing, source location and relative intensity. However, the lack of direct measurements of dust emissions makes a complete validation of the simulated dust fluxes impossible.

Over the 6 yr of simulations, three main source regions contribute almost equally to 98% of the average annual emissions: the Taklimakan, the northern deserts of China and the Gobi desert. However, their contributions to the total number of dust emission events are significantly different. The Taklimakan desert is the most frequent dust source (59% of the dust emission events). On the contrary, only 2% of the total dust events originate from the Gobi desert, but these few events can represent a major part of the annual mass of emitted dust. On average, the northern deserts of China contribute almost equally (~35%) to the total number of dust emission events and to the annual mass of emitted dust but with a significant inter-annual variability.

The seasonal cycle of dust event frequencies is well reproduced, with a maximum of dust emission events occurring in spring. This seasonal cycle is mainly controlled in latter spring and in the summer by the emissions occurring in the Taklimakan desert, and in the winter by those occurring in the northern deserts of China. A very high inter-annual variability of the dust emissions is simulated, mainly due to large and sporadic emissions from the Gobi desert and, to a lesser extent, from the northern deserts of China. The simulated annual dust emissions vary within a factor of about 5. Soil moisture and snow cover do not affect significantly neither the seasonal cycle nor the inter-annual variability of the dust emissions. They can decrease the winter dust emissions by 80 to 95%. However, during the spring, i.e., the most intense period of dust emissions, their influence is relatively weak (~5.5%).

Significant uncertainties remain concerning the simulations of dust emissions for eastern Asia since the differences between simulations performed by different models is up to 50%. In our case, the uncertainties are likely due to the lack of precise maps of surface features (especially for the soil clay content and the erodible fraction of the surface) and to the

uncertainty on the meteorological data (especially wind velocity fields). Moreover, some surface parameters not accounted for in these studies, such as soil crusting or supply limitation, would require complementary investigations. Lastly, the lack of direct estimations of dust emissions clearly limits our abilities to go further in dust emissions modelling over China and Mongolia. In situ measurements performed for representative surfaces (sandy and gobi deserts) in the main source areas are really needed to quantify precisely the dust emissions from the different dust source areas of eastern Asia.

Acknowledgments

We would like to thank Elisabeth Bon Nguyen for allowing the adaptation of the map of Chinese and Mongolian deserts.

References

Alfaro, S.C., Gomes, L., 2001. Modeling mineral aerosol production by wind erosion: emission intensities and aerosol distributions in source areas. J. Geophys. Res. 106, 18,075–18,084.

Betts, A.K., Beljaars, A.C.M., 2003. ECMWF ISLSCP-II near-surface dataset from ERA-40. ERA-40 Project Report Series from ECMWF, vol. 8. 31 pp.

Callot, Y., Marticorena, B., Bergametti, G., 2000. Geomorphologic approach for modelling the surface features of arid environments in a model of dust emissions: application to the Sahara desert. Geodin. Acta 13, 245–270.

Chatenet, B., Marticorena, B., Gomes, L., Bergametti, G., 1996. Assessing the microped size distributions of desert soils erodible by wind. Sedimentology 43, 901–911.

Ding, Z.L., Ren, J.Z., Yang, S.L., Liu, T.S., 1999. Climate instability during the penultimate glaciation: evidence from two high-resolution loess records, China. J. Geophys. Res. 104, 20,123–20,132.

Fécan, F., Marticorena, B., Bergametti, G., 1999. Parameterization of the increase of the aeolian erosion threshold wind friction velocity due to soil moisture for semi arid areas. Ann. Geophys. 17, 149–157.

Gao, T., Yu, X., Ma, Q., Li, H., Li, X., Si, Y., 2003. Climatology and trends of the temporal and spatial distribution of sandstorms in Inner Mongolia. Water Air Soil Pollut. 3, 51–66.

Gillette, D.A., 1979. Environmental factors affecting dust emission by wind erosion. In: Morales, C. (Ed.), Saharan Dust. Wiley and Sons, New York, USA, pp. 71–94.

Gillette, D.A., 1981. Production of dust that may be carried great distances, Desert Dust: origin, characteristics and effect on man. Spec. Pap.-Geol. Soc. Am. 186, 11–26.

Gillette, D.A., Adams, J., Muhs, D.R., Khil, R., 1982. Threshold friction velocities and rupture moduli for crusted desert soils for the input of soil particles into the air. J. Geophys. Res. 87, 9003–9015.

Gomes, L., Bergametti, G., Coudé-Gaussen, G., Rognon, P., 1990. Submicron desert dust: a sandblasting process. J. Geophys. Res. 95, 13927–13935.

Gong, S.L., Zhang, X.Y., Zhao, T.L., McKendry, I.G., Jaffe, D.A., Lu, N.M., 2003. Characterization of soil dust aerosol in China and its transport and distribution during 2001 ACE-Asia: 2. Model simulation and validation. J. Geophys. Res. 108, 4262. doi:10.1029/2002JD002633.

Greeley, R., Blumberg, D.G, McHone, J.F., Dobrovolski, A., Iversen, J., Lancaster, N., Rasmussen, K.R., Wall, S., White, B., 1997. Applications of spaceborne radar laboratory data to the study of aeolian processes. J. Geophys. Res. 102, 10,971–10,983.

Husar, R.B., Tratt, D.M., Schichtel, B.A., Falke, S.R., Li, F., Jaffe, D., Gassó, S., Gill, T., Laulainen, N.S., Lu, F., Reheis, M.C., Chun, Y., Westphal, D., Holben, B.N., Gueymard, C., McKendry, I., Kuring, N., Feldman, G.C., McClain, C., Frouin, R.J., Merrill, J., Dubois, D., Vignola, F., Murayama, T., Nickovic, S., Wilson, W.E., Sassen, K., Sugimoto, N., Malm, W.C., 2001. Asian dust events of April 1998. J. Geophys. Res. 106, 18,317–18,330.

In, H.J., Park, S.U., 2002. A simulation of long range transport of yellow sand observed in April 1998 in Korea. Atmos. Environ. 36, 4173–4187.

Iversen, J.D., White, B.R., 1982. Saltation threshold on Earth, Mars and Venus. Sedimentology 29, 111–119.

Kurosaki, Y., Mikami, M., 2003. Recent frequent dust events and their relation to surface wind in East Asia. Geophys. Res. Lett. 30 (14), 1736. doi:10.1029/2003GL017261.

Laurent, B., Marticorena, B., Bergametti, G., Chazette, P., Maignan, F., Schmechtig, C., 2005. Simulation of the mineral dust emission frequencies from desert areas of China and Mongolia using an aerodynamic roughness length map derived from the POLDER/ADEOS 1 surface products. J. Geophys. Res. 110, D18S04. doi:10.1029/2004JD005013.

Liu, M., Westphal, D.L., Wang, S., Shimizu, A., Sugimoto, N., Zhou, J., Chen, Y., 2003. A high numerical study of the Asian dust storms of April 2001. J. Geophys. Res. 108. doi:10.1029/2002JD003178.

Lopez, M.V., 1998. Wind erosion in agricultural soil: an example of limited supply of particles available for erosion. Catena 33, 17–28.

Mainguet, M., 1996. Aridité, sécheresse et dégradation dans les aires sèches de Chine. Sécheresse 7, 41–50.

Marticorena, B., Bergametti, G., 1995. Modeling the atmospheric dust cycle: 1. Design of a soil derived dust production scheme. J. Geophys. Res. 100, 16415–16430.

Marticorena, B., Bergametti, G., Aumont, B., Callot, Y., N'Doumé, C., Legrand, M., 1997a. Modeling the atmospheric dust cycle: 2. Simulations of Saharan dust sources. J. Geophys. Res. 102, 4387–4404.

Marticorena, B., Bergametti, G., Gillette, D.A., Belnap, J., 1997b. Factors controlling threshold friction velocity in semiarid and arid areas of the United States. J. Geophys. Res. 102, 23277–23287.

Marticorena, B., Chazette, P., Bergametti, G., Dulac, F., Legrand, M., 2004. Mapping the aerodynamic roughness length of desert surfaces from the POLDER/ADEOS bi-directional reflectance product. Int. J. Remote Sens. 25 (3), 603–626.

Mc Kenna-Neuman, C., Nickling, W.G., 1994. Momentum extraction with saltation: implications for experimental evaluation of wind profile parameters. Boundary-Layer Meteorol. 68, 35–50.

Mei, F., Zhang, X., Lu, H., Shen, Z., Wang, Y., 2004. Characterization of MASDs of surface soils in north China and its influence on estimating dust emission. Chin. Sci. Bull. 49 (20), 2169–2176.

Merrill, J.T., Uematsu, M., Bleck, R., 1989. Meteorological analysis of long-range transport of mineral aerosols over the North Pacific. J. Geophys. Res. 94, 8584–8598.

Middleton, N.J., 1989. Climatic controls on the frequency, magnitude and distribution of dust storms: examples from India/Pakistan, Mauritania and Mongolia. In: Leinen, M., Sarnthein, M. (Eds.), Paleoclimatology and Paleometeorology: Modern and Past

Patterns of Global Atmospheric Transport. Kluwer Academic Publ., Dordrecht, pp. 97–132.
Mitchell, D.J., Fullen, M.A., 1994. Soil-forming processes on reclaimed desertified land in north-central China. In: Milington, A.C., Pye, K. (Eds.), Environmental Change in Drylands: Biogeographical and Geomorphological Perspectives. J. Wiley, pp. 393–412.
Mougin, E., Lo Seen, D., Rambal, S., Gaston, A., Hiernaux, P., 1995. A regional sahelian grassland model to be coupled with multispectral satellite data: I. Model description and validation. Remote Sens. Environ. 52, 191–193.
Natsagdorj, L., Jugder, D., Chung, Y.S., 2003. Analysis of dust storms observed in Mongolia during 1937–1999. Atmos. Environ. 37, 1401–1411.
Nickling, W.G., Gillies, J.A., 1989. Emission of fine-grained particulates from desert soils. In: Leinen, M., Sarnthein, M. (Eds.), Paleoclimatology and Paleometeorology: Modern and Past Patterns of Global Atmospheric Transport. Kluwer Academic Publ., Dordrecht, pp. 133–165.
Qian, W., Quan, L., Shi, S., 2002. Variations of the dust storm in China and its climatic control. J. Climate 15, 1216–1229.
Shao, Y., Raupach, M.R., Findlater, P.A., 1993. Effect of saltation bombardment on the entrainment of dust by wind. J. Geophys. Res. 98, 12719–12726.
Shao, Y., Yang, Y., Wang, J., Song, Z., Leslie, L.M., Dong, C., Zhang, Z., Lin, Z., Kanai, Y., Yabuki, S., Chun, Y., 2003. Northeast Asian dust storms: real-time numerical prediction and validation. J. Geophys. Res. 108, 4691. doi:10.1029/2003JD003667.
Sörensen, M., 1985. Estimation of some aeolian saltation transport parameters from transport rate profiles. In: Barndorff-Nielsen, O.E., Möller, J.T., Römer Rasmussen, K., Willets, B.B. (Eds.), Proceedings of the International Workshop on the Physics of Blown Sand. University of Aarhus, Aarhus, Denmark, pp. 141–190.
Sun, J., Zhang, M., Liu, T., 2001. Spatial and temporal characteristics of dust storms in China and its surrounding regions, 1960–1999: relations to source area and climate. J. Geophys. Res. 106, 10,325–10,333.
Sun, L., Zhou, X., Lu, J., Kim, Y.P., Chung, Y.S., 2003. Climatology, trend analysis and prediction of sandstorms and their associated dustfall in China. Water Air Soil Pollut. 3, 41–50.
Uno, I., Amano, H., Emori, S., Kinoshita, K., Matsui, I., Sugimoto, N., 2001. Trans-Pacifique yellow sand transport observed in April 1998: a numerical simulation. J. Geophys. Res. 106, 18,331–18,344.
Uppala, S., Kållberg, P., Hernandez, A., Saarinen, S., Fiorino, M., Li, X., Onogi, K., Sokka, N., Andrae, U., Da Costa-Bechtold, V., 2004. ERA-40: ECMWF 45-year reanalysis of the global atmosphere and surface conditions 1957–2002. In: White, Peter (Ed.), ECMWF Newsletter, vol. 101. Shinfield Park, Reading, Berkshire RG2 9AX, UK.
Van Den Hurk, B., Viterbo, P., Beljaars, A., Betts, A., 2000. Offline validation of the ERA-40 surface scheme, ECMWF Technical Memorandum, 295, European Center for Medium-range Weather Forecasts, Shinfield Park, Reading RG2 9AX, UK. 43 pp.
Walker, A.S., 1986. Eolian landforms (chapter 8). In: Short, N.M., Blair, R.W. (Eds.), Geomorphology from Space: A Global Overview of Regional Landforms. NASA Publication.
Wang, Z., Ueda, H., Huang, M., 2000. A deflation module for use in modeling long-range transport of yellow sand over East Asia. J. Geophys. Res. 105, 26,947–26,959.
Wang, X., Ma, Y., Chen, H., Wen, G., Chen, S., Tao, Z., Chung, Y.S., 2003. The relation between sandstorms and strong winds in Xinjiang, China. Water Air Soil Pollut. 3, 67–79.
Webb, R.W., Rosenzweig, C.E., Levine, E.R., 2000. Global Soil Texture and Derived Water-Holding Capacities. Oak Ridge National Laboratory Distributed Active Archive Center, Oak Ridge, TN, USA.
White, B.R., 1979. Soil transport by winds on Mars. J. Geophys. Res. 84, 4643–4651.
Williams, G., 1964. Some aspects of the aeolian saltation load. Sedimentology 3, 253–256.
Xian, X., Tao, W., Qingwei, S., Weimin, Z., 2002. Field and wind-tunnel studies of aerodynamic roughness length. Boundary-Layer Meteorol. 104, 151–163.
Xue, Y., 1996. The impact of desertification in the Mongolian and the Inner Mongolian grassland on the region climate. J. Climate 9, 2173–2189.
Yang, G.., Xiao, H., Tuo, W., 2001. Black windstorm in northwest China: a case study of the strong sand-dust storm on May 5th 1993. Global Alarm: Dust and Sandstorms from the World's Drylands, Report of United Nations, 2001, pp. 49–73.
Zender, C.S., Miller, R., Tegen, I., 2004. Quantifying Mineral Dust Mass Budgets: Terminology, Constraints, and Current Estimates, Eos, vol. 85(48). Eos, pp. 509–512.
Zha, Y., Gao, J., 1997. Characteristics of desertification and its rehabilitation in China. J. Arid Environ. 37, 419–432.
Zhang, X.Y., Arimoto, R., An, Z.S., 1997. Dust emission from Chinese desert sources linked to variations in atmospheric circulation. J. Geophys. Res. 102, 28,041–28,047.
Zhang, X.Y., Gong, S.L., Zhao, T.L., Arimoto, R., Wang, Y.Q., Zhou, Z.J., 2003. Sources of Asian dust and role of climate change versus desertification in Asian dust emission. Geophys. Res. Lett. 30, 2272. doi:10.1029/2003GL018206.
Zhao, T.L., Gong, S.L., Zhang, X.Y., McKendry, I.G., 2003. Modeled size-segregated wet and dry deposition budgets of soil dust aerosol during ACE-Asia 2001: implications for Trans-Pacific transport. J. Geophys. Res. 108, 8665. doi:10.1029/2002JD003363.
Zhao, T.L., Gong, S.L., Zhang, X.Y., McKendry, I.G., Zhou, Z., 2004. A simulated climatology of Asian dust aerosol and its trans-pacific transport: mean climate and validation. International Symposium on Sand and Dust Storm, Beijing, China, p. 143.
Zobler, L., 1986. A world soil file for global climate modeling. NASA Tech. Memo. 87802.